Journal of
Marine Science
and Engineering

MDPI

Article

Effect of High Temperature on Mechanical Properties and Microstructure of HSFCM

Yanbin Li [1], Qingsheng Meng [1,*], Yan Zhang [2,*], Huadong Peng [3] and Tao Liu [1,4]

[1] Shandong Provincial Key Laboratory of Marine Environment and Geological Engineering, Ocean University of China, Qingdao 266100, China; li117156@163.com (Y.L.)
[2] College of Civil Engineering, Anhui Jianzhu University, Hefei 230601, China
[3] Shanghai Survey, Design and Research Institute (Group) Co., Ltd., Qingdao 266100, China
[4] Qingdao National Laboratory of Marine Science and Technology, Qingdao 266000, China
* Correspondence: qingsheng@ouc.edu.cn (Q.M.); avayan8006@163.com (Y.Z.)

Abstract: A new type of composite cement-based cementing material—high-strength fast cementing material (HSFCM)—will be widely used in marine engineering projects such as submarine tunnels. However, the influence of fire and other high temperature conditions on its material properties have not been explored in previous studies. Mechanical tests and microstructure observations of HSFCM were carried out, and the strength and deformation characteristics, microstructure and composition evolution of HSFCM after high temperature treatment were discussed. After high temperature treatment, the compressive strength of HSFCM deteriorated. The compressive strength of HSFCM decreased by more than half at 400 °C. The peak strain increased at 200 °C with the increase of temperature, and decreased at 400~600 °C with the increase of temperature. High temperature reduces the stiffness of HSFCM, and the elastic modulus decreases with increasing temperature. The influence of high temperature on the microstructure of HSFCM is mainly shown in the increase and enlargement of pores in three-dimensional space, the development of micro-cracks and the thermal decomposition of cementing material into stable oxides without cementing effect. The microscopic changes of HSFCM are in good agreement with the mechanical test results.

Keywords: cement-based material; high temperature; indoor test; mechanical properties; microanalysis

Citation: Li, Y.; Meng, Q.; Zhang, Y.; Peng, H.; Liu, T. Effect of High Temperature on Mechanical Properties and Microstructure of HSFCM. *J. Mar. Sci. Eng.* **2023**, *11*, 721. https://doi.org/10.3390/jmse11040721

Academic Editor: Cristiano Fragassa

Received: 10 March 2023
Revised: 24 March 2023
Accepted: 25 March 2023
Published: 27 March 2023

1. Introduction

Coastal areas are the most economically developed areas in China, with numerous engineering projects [1] and huge uses of cement-based cementing materials [2]. Currently, cement-based materials are widely used in offshore projects, such as undersea tunnel construction [3], offshore oil and gas engineering [4], submarine pipeline construction [5] and offshore bridge construction [6]. Taking Qingdao, a coastal city in northern China, as an example, with the expansion of the construction scope of urban public transport facilities in recent years, the number of undersea tunnels in this area is increasing (as shown in Figure 1A). Cementing materials are widely used in weak strata reinforcement, concrete lining reinforcement, surrounding rock plugging and other conditions (as shown in Figure 1B). The performance of cementing materials directly affects the stability and durability of supporting structures and surrounding rock strata. The increased construction in the area has increased the risk of accidents such as fire. As the undersea tunnel is a narrow and closed structure located in the underwater environment, fire often causes heavy casualties and huge economic losses. At the same time, due to the poor ventilation of undersea tunnels, fire can cause the ambient temperature to reach more than 1000 °C [7]; high temperatures will affect the structural composition of cement-based cementing material, changing the mechanical properties of the material, causing the tunnel structure to crack and affecting the bearing capacity and service life of the undersea tunnel. This can lead to tunnel collapse, threatening the safety and stability of the project [3,8–10].

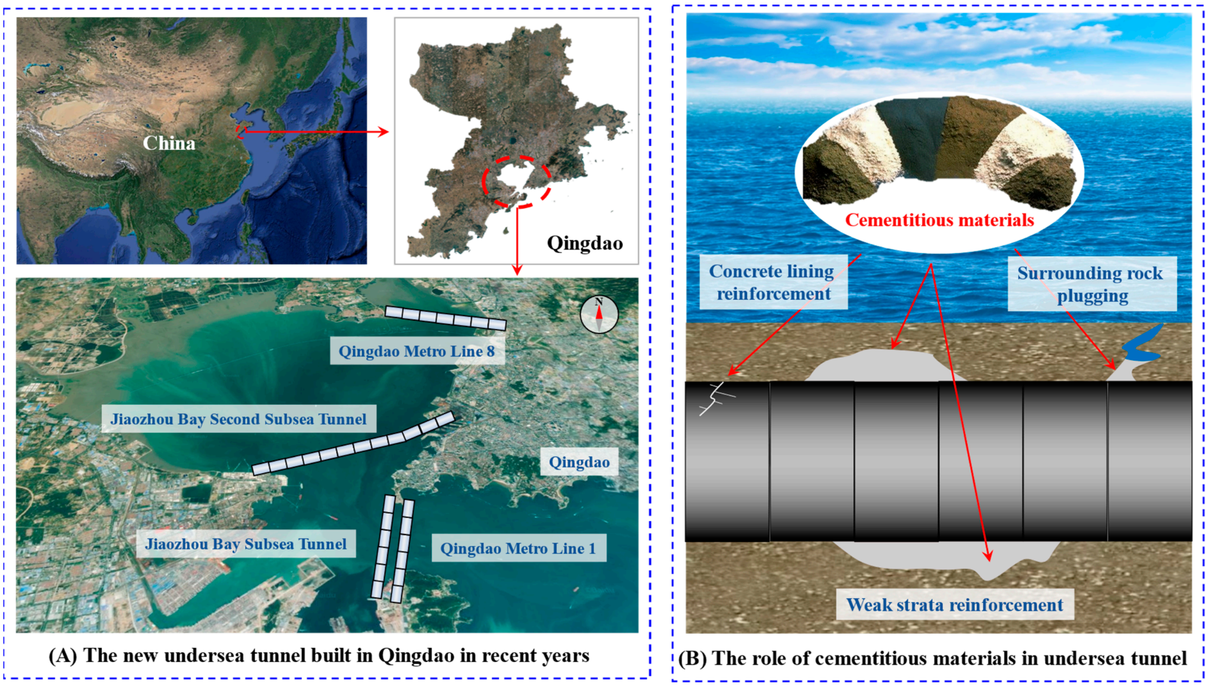

Figure 1. The role of cement-based cementitious materials in growing marine engineering.

It is very important to study the evolution law and mechanism of properties of cement-based cementitious materials at high temperature for accurate evaluation of engineering structure safety and further improvement of material properties. Portland cement is a widely used basic cementing material. When exposed to the influence of a high temperature environment, the hue of its surface color will change, accompanied by volume change and damage [11]. Observation of the microstructure revealed that thermal cracking between different media was the main reason for performance degradation [12]. In some emergency projects, aluminate series cement with shorter curing time is used, and its performance is more significantly affected by high temperature [13–15]. A variety of composite cementing materials have been developed based on cement. The bearing capacity of engineering cementing composites (ECC) is reduced at high temperature [16]. The specimen size does not affect the percentage of strength loss [17]. Fiber can be added to obtain higher toughness [18]; recycled materials such as alkali slag and fly ash are also often used to improve high temperature resistance of cement-based cementitious materials, and obtaining the law of mechanical properties changing with temperature [19,20]. With the development of experimental techniques and equipment, the mechanism of microstructure change of cement-based materials after high temperature has been revealed by various means [21–23].

Due to the particularity and complexity of the location, the construction cost of marine engineering is often very high. The key to saving investment is to use the appropriate construction technology and cementing materials to reduce the construction period [24]. At present, Portland cement is mainly used in marine engineering in China, but its single property, poor durability such as impermeability, corrosion resistance and freeze–thaw resistance, cannot fully meet the special requirements of marine engineering [25]. Different types of cementing materials have different engineering properties. For construction projects in coastal areas that require materials to set quickly and become strong early, our predecessors developed a new high-strength fast cementing material, HSFCM [26], which is a composite cement-based cementitious material. It is often used in grouting engineering to reinforce the weak stratum and lining structure, which can significantly shorten the site construction period [27], and it has a wide application prospect. However, there are few studies on HSFCM at present. Most of these studies were conducted at normal temperature, aiming at the engineering characteristics of the anchorage structure. This makes it is impossible to evaluate the influence of high temperature on this material, which restricts its wider application. Therefore, focusing on the influence of high temperature on HSFCM and studying the evolution law and mechanism of its mechanical properties can provide an important reference for evaluating the properties of materials and further improving materials.

2. Materials and Methods

2.1. Materials and Specimen Preparation

The material used in this study is HSFCM, a composite cement-based cementitious material produced by a company in Shandong Province. The composition of the raw materials is shown in Table 1 [26].

Table 1. The raw materials composition of HSFCM.

Material	Proportion (wt%)
Sulfoaluminate cement	30~50%
Early strength Portland cement	15~25%
Fine sand	25~35%
Calcium sulfate	3~7%
Calcium carbonate	3~7%
Magnesium oxide	0.7~1.3%
Silicon powder	0.7~1.3%
Water reducer	0.7~1.3%
Boric acid	0.07~0.13%

The particle size distribution of cement-based cementitious materials is closely related to their mechanical properties [28]. Particle size analysis of HSFCM was carried out using a Winner 3003 dry laser particle size analyzer, and the particle size distribution curve is obtained as shown in Figure 2. It can be seen that the particle size distribution of HSFCM is uneven, most of the particle size is concentrated in the range of 10~40 μm, particles at the size of about 100 μm are few and the material is poorly graded.

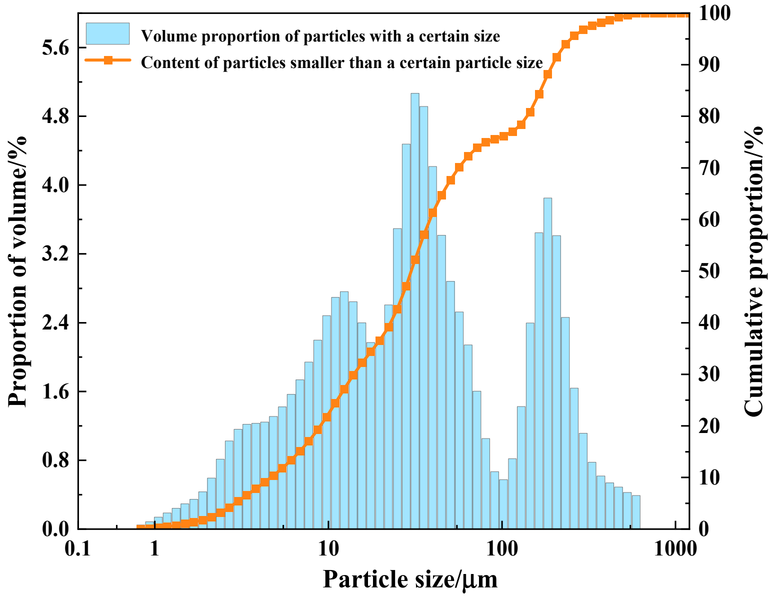

Figure 2. Particle size distribution of HSFCM.

HSFCM is often used as a grouting material in marine engineering. The diffusion capacity of the material can be measured by indicators such as fluidity and setting time. The differences in performance between HSFCM and Portland cement commonly used in marine engineering were compared through laboratory tests. The materials were weighed with the water/material ratio of 0.3 [26,27]. The stirred HSFCM and Portland cement were filled with the cup–cone round mold, respectively, and then the mold was lifted to let the slurry flow freely until it stopped under the condition of no disturbance. The diffusion diameter was measured with calipers to calculate the fluidity. Use Vicat apparatus to measure the setting time, when measuring let the test needle freely sink into the pure pulp, observe the pointer reading and obtain the final setting time. The mobility and setting time data are shown in Table 2. Under the same water–material ratio, HSFCM fluidity is obviously greater than Portland cement, HSFCM water requirement is smaller and the grouting diffusion range is larger. Furthermore, HSFCM setting time is shorter than Portland cement. HSFCM can set and harden faster to achieve strength, which is conducive to the next early process.

Table 2. Comparison of HSFCM and Portland cement grouting properties.

Indicators	HSFCM	Portland Cement
Fluidity (cm)	**35**	**6**
Final setting time (min)	**80**	**375**

Cylindrical specimens with a diameter of 50 mm and a length-to-diameter ratio of 2.0 were produced for the test according to ASTM C39 recommended dimensional standards [29]. The mixing procedure: HSFCM was poured into a mixing bucket and stirred for 1 min, then mixed with water according to the water/material ratio of 0.3. The mixing was continued for 5 min and then the mixture was injected into the mold prepared in advance, vibrated and then left to stand for 24 h at room temperature before demolding, and then placed in a standard maintenance room at a temperature of (20 ± 3) °C and relative humidity of (95 ± 2)% for 28 d.

2.2. Test Procedure

The GR.AF80/14 atmosphere furnace was used for high temperature treatment of the specimens, and the heating temperature was set to 100 °C, 150 °C, 200 °C, 400 °C and 600 °C for five test groups. The specimens at room temperature (20 °C) were used as the control group. In order to ensure that the specimens were uniformly heated, the heating rate was set to 5 °C/min, and the rated temperature was maintained for 4 h (Figure 3A). Then the heating was stopped and the specimens were taken out after natural cooling in the chamber (Figure 3B).

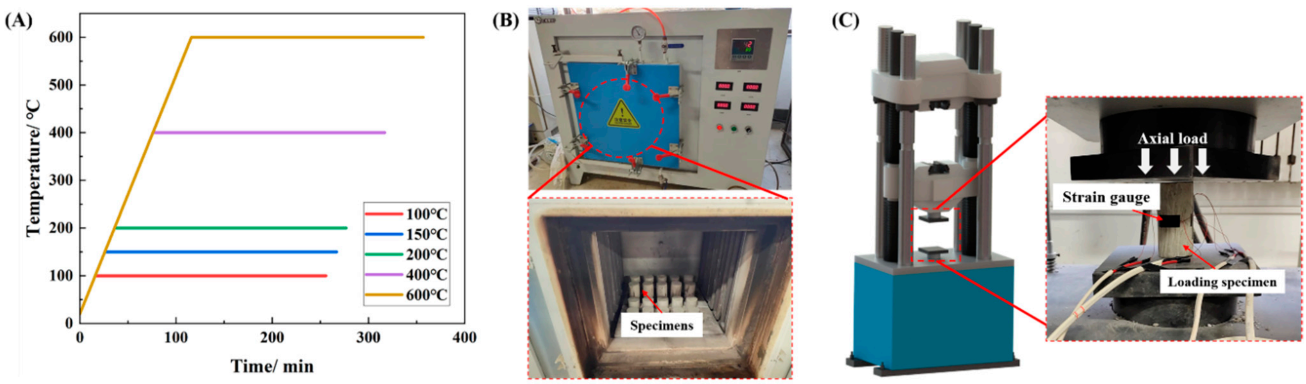

Figure 3. Temperature rise curve (**A**), high temperature treatment equipment (**B**) and test device for uniaxial compression (**C**).

The SHT4106 electro-hydraulic servo-type instrument was used to test the mechanical properties of the specimens after high temperature treatment. The axial displacement-controlled loading mode with a loading rate of 0.5 mm/min was selected. The arrangement of the device is shown in Figure 3C. The microstructure and morphological evolution of

HSFCM were analyzed by a nanoVoxel-2792 X-ray three-dimensional microscopic imaging system and a scanning electron microscope. At the same time, HSFCM specimens were selected for an XRD test, and the diffraction profile was obtained by MDI Jade software to analyze the changes in microscopic composition.

3. Results

3.1. Uniaxial Compression Test

3.1.1. Compressive Strength

Compressive strength, which is closely related to elastic modulus, peak strain and other mechanical parameters, is the most conventional and important index for testing mechanical properties of materials [30]. A uniaxial compression test was conducted on HSFCM specimens treated by atmosphere furnace. Figure 4 shows the compressive strength of HSFCM treated at different temperatures.

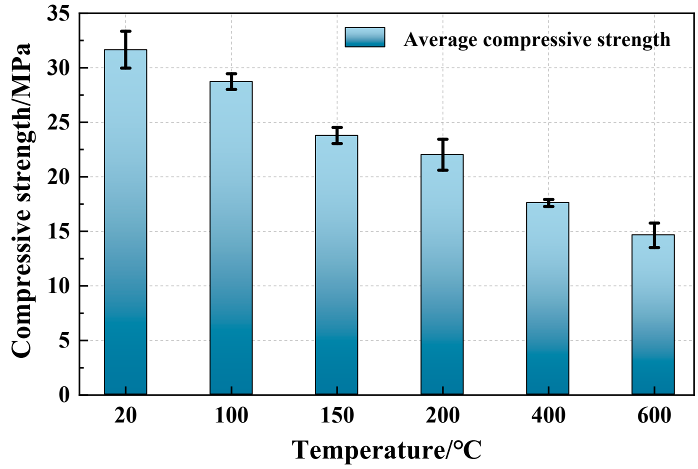

Figure 4. Compressive strength of HSFCM after treatment at different temperatures.

High temperature deteriorates the compressive strength of HSFCM. The average compressive strength of specimens treated at 100 °C, 150 °C, 200 °C, 400 °C and 600 °C was 28.73 MPa, 23.78 MPa, 22.02 MPa, 17.60 MPa and 14.64 MPa, respectively. Compared with 31.65 MPa at 20 °C, the compressive strength decreased by 9.24%, 24.87%, 30.43%, 44.39% and 53.75%, respectively. It can be seen that the compressive strength of HSFCM gradually decreased with the increase in temperature. At 100 °C, the compressive strength decreased less, the specimens were in the stage of free water evaporation in the internal pores and the internal damage was relatively light. At 100~200 °C, the free water in the specimens completely evaporated, the internal damage was aggravated and the strength decreased rapidly. When the temperature rose above 400 °C, a large number of hydration products were dehydrated, the cement matrix was heated and cracked and the internal micro-cracks expanded. At this time, the compressive strength could be reduced by more than half.

3.1.2. Stress–Strain Curve

The stress–strain relationship reflects the most basic mechanical properties of materials and is the main basis for studying mechanical strength and deformation characteristics [31]. Figure 5 shows the compressive stress–strain characteristic curve of HSFCM after high temperature.

After high temperature treatment, the compressive stress–strain curve of HSFCM can be divided into four stages: compression and compact section, elastic growth section, yield section and residual section. At the initial stage of compression, the specimen stiffness increases due to the external force compaction of the internal pores, and the curve presents an upward concave shape. When the strain reaches 20% of the peak strain of the specimen, the approximate linear growth of the curve indicates that the elastic growth stage is entered. As the loading continues, the curve no longer increases linearly; at this time, the internal damage of the specimen intensifies, and the curve becomes concave downward into the yield section until the specimen's brittle failure occurs at the peak, and the curve drops sharply. After that, the compressive stress does not increase and the strain increases, entering the residual section. With the increase of temperature, the peak stress and curve slope decrease, and the growth segment before reaching the peak stress decreases. It is particularly noted that after the specimens were treated at 400~600 °C, the color gradually deepened, the mesh cracks appeared on the surface and gradually expanded and some specimens burst, indicating that the HSFCM specimen had local damage between 400~600 °C. This is also the reason for the change of the peak strain trend of the specimen at 400~600 °C. Due to the already existing failure in the specimen after the high temperature treatment, when a small strain occurs in compression of the specimen, it will be reflected as compression failure. Therefore, at 400~600 °C, the stress–strain curve does not reflect the whole process of specimen failure, but only the process of compression failure.

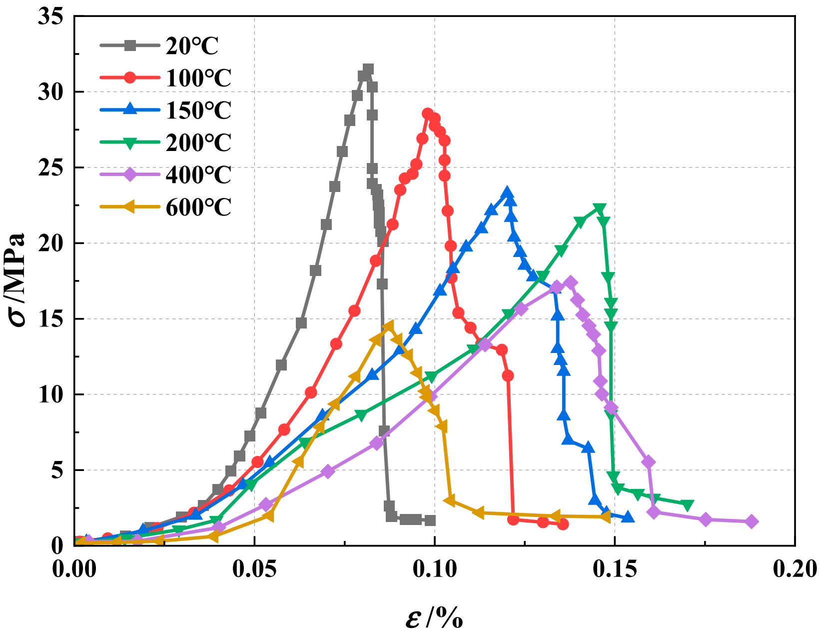

Figure 5. Compressive stress–strain curve of HSFCM after treatment at different temperatures.

3.2. CT Scan of Pore Structure

The macroscopic mechanical properties of cementitious materials depend on the stability and density of the internal microstructure. The thermal decomposition of cementitious materials at high temperature will cause the change of the internal microstructure, resulting in the deterioration of the macroscopic mechanical properties [21,32,33].

The same HSFCM specimen was selected for CT scanning in order to obtain the changes of the microscopic pore structure of the material with temperature. Firstly, a cylindrical specimen with a diameter of 50 mm and a length of 100 mm was prepared, which was drilled and polished into a cylindrical specimen with a diameter of 3 mm and a length of 10 mm for CT scanning. The specimen was scanned in a CT device to obtain fluoroscopic images. After that, the specimen was transferred to the atmosphere furnace for high temperature treatment. After natural cooling, CT scanning was carried out to obtain the images of the specimen treated at 100 °C and 400 °C, successively. After the scanning, the software supporting the instrument was used to reconstruct the overall and internal morphology of the specimen, and the influence of temperature on the microstructure was analyzed by analyzing gray decay and three-dimensional pore structure changes.

Figure 6 shows CT scanning images of different cross sections (n_z = 300 layers, 600 layers, 900 layers), longitudinal sections (n_x = 450 layers) and three-dimensional pore distribution of the specimen treated at 20 °C, 100 °C and 400 °C. The images were rendered—the higher the density, the whiter and brighter the image color—and a threshold segmentation method was used to obtain the distribution of pores within the specimen, marked in red.

By comparison, it can be seen that the influence of high temperature treatment on HSFCM is mainly manifested as the increase in the number of pores and the size of pores in the three-dimensional space. The distribution of pores in the specimen at 100 °C is little different from that at 20 °C, but the number of pores increases, mainly distributed in the top and middle of the specimen, and a large number of coarse particles such as fine sand are distributed at the bottom. At 400 °C, the internal pores of the specimen increased significantly, and with the increase of temperature, the high-density material at the bottom also gradually experienced thermal decomposition. The changes of micro-pores are in good agreement with the evolution of macro-mechanical properties.

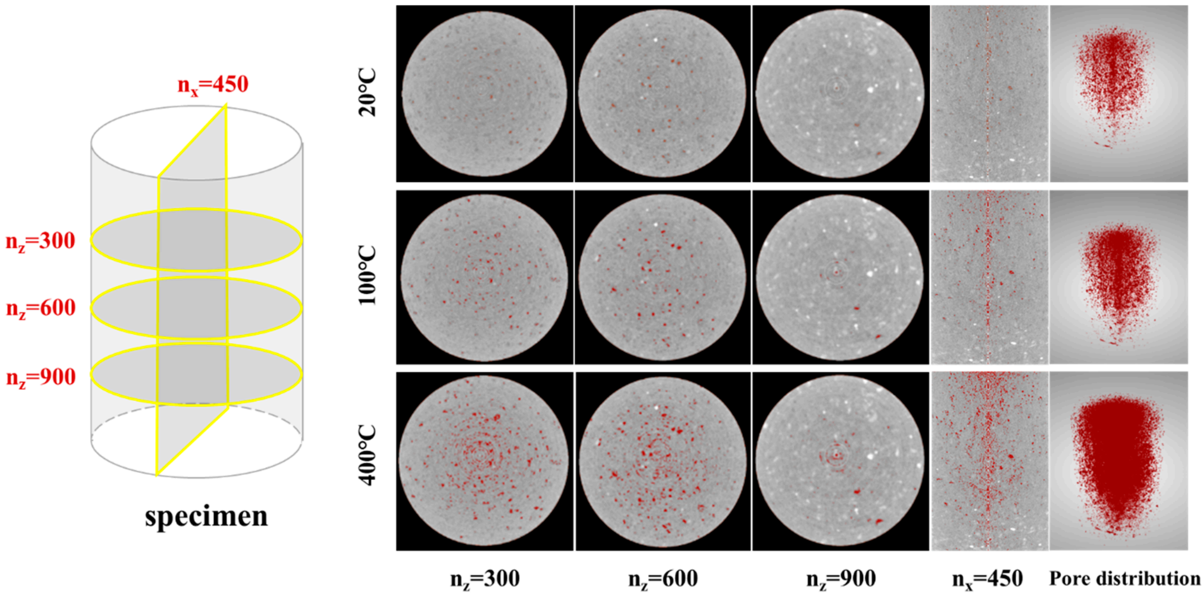

Figure 6. CT images of different sections and internal pores of HSFCM.

3.3. Component Analysis

High temperature deterioration of cement-based cementitious materials is not only a physical process, but also a chemical reaction of composition change [34–36]. Therefore, an X-ray diffraction test (XRD) was used to discuss the composition change under the condition of thermal decomposition of materials, and the XRD pattern as shown in Figure 7 was obtained.

As seen in Figure 7, the XRD pattern of HSFCM changes after high temperature treatment. Multiple ettringite and calcium silicate hydrate diffraction peaks can be identified at 20 °C. The reason why HSFCM can coagulate quickly and become strong early is that it contains a large number of active silica substances, which can react with $Ca(OH)_2$ to form calcium silicate hydrate gels ($CaO{\cdot}SiO_2{\cdot}nH_2O$, C-S-H), etc. Such substances are the products of a hydration reaction. It reflects the main bonding substance in the specimen. When it rises to 100 °C, the diffraction peaks of ettringite decrease obviously, and multiple $CaSO_4$ diffraction peaks appear, indicating that the decomposition of ettringite occurs under heat. The diffraction peaks of calcium silicate hydrate are slightly enhanced, and the diffraction peaks of SiO_2 and $Ca(OH)_2$ are slightly reduced, indicating that the remaining SiO_2 and $Ca(OH)_2$ in the specimen continue to undergo hydration reactions to produce hydration products before the free water evaporates completely. When the temperature exceeds 400 °C, the diffraction peaks of ettringite and calcium silicate hydrate almost disappear, and multiple diffraction peaks of SiO_2 and $CaSO_4$ appear again, indicating that hydration products are further decomposed by heat with the increase in temperature. In addition, multiple diffraction peaks of CaO appear, which may be the CaO generated by the heat dehydration of $Ca(OH)_2$ and the heat decomposition of $CaCO_3$. On the whole, with the increase in treatment temperature, the decomposition of gelling substances in HSFCM becomes more serious, and stable oxides without gelling are eventually generated, resulting in serious deterioration of material properties.

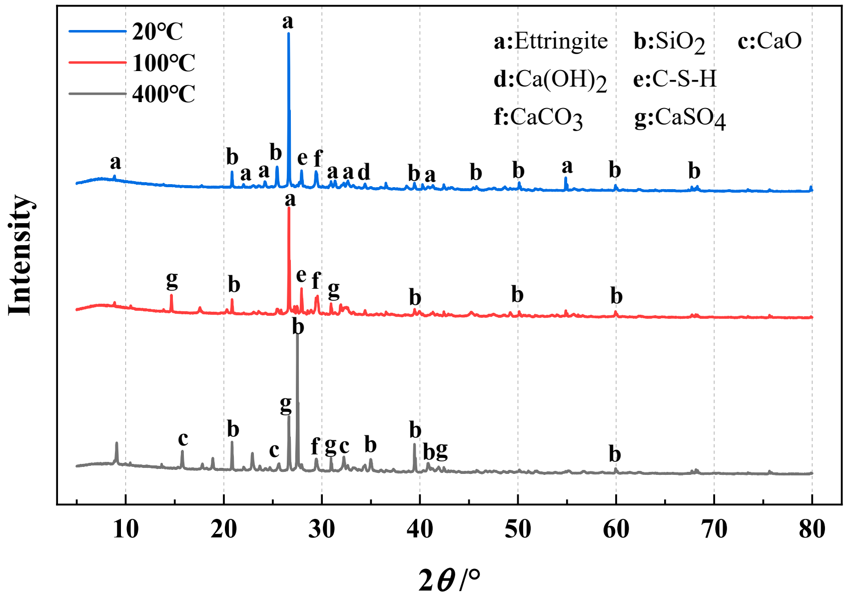

Figure 7. XRD pattern of HSFCM after treatment at different temperatures.

3.4. Surface Morphology Analysis

In order to more directly observe the changes in the surface microstructure of HSFCM, a scanning electron microscope (SEM) was used for observation and analysis, and the scanning images are shown in Figure 8.

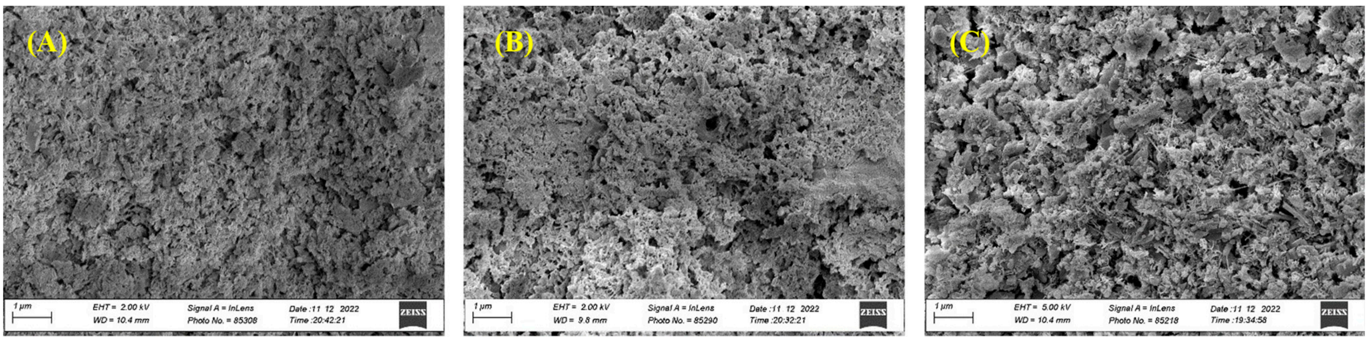

Figure 8. SEM images of HSFCM after treatment at 20 °C (**A**), 100 °C (**B**) and 400 °C (**C**).

The surface of the HSFCM specimen without high temperature treatment is more uniform and flat; the number of pores and micro-cracks is less; the hydration products grow freely; there are $Ca(OH)_2$, ettringite crystals and C-S-H gels, etc.; the contact between particles is close; the bonding degree is higher; and the microstructure is good. When the temperature is 100 °C, the surface is slightly convex; the fold becomes rough; the size and number of pores increase, but no obvious crack development has occurred; and the degree of bonding of the gel becomes low. At 400 °C, a large number of irregular crystals and whiskers appear; the bonding substance between the crystals is reduced; the specimen surface becomes uneven; the honeycomb micro-pores increase; the pore structure increases; and the micro-cracks develop through each other, which is consistent with the results of CT scanning and XRD analysis.

4. Discussion

4.1. Comparison of Compressive Strength with Other Cementitious Materials

The ratio of compressive strength of HSFCM after high temperature treatment f_c^T to compressive strength at room temperature f_c^{20} was selected and compared with silicate cement PO [37], engineering cementitious composites ECC [17], calcium aluminate cement CAC [38], magnesium potassium phosphate cement MKPC [39] and strain-hardening cementitious composites with high-volume of fly ash HVFA-SHCC [20] for comparison (Figure 9).

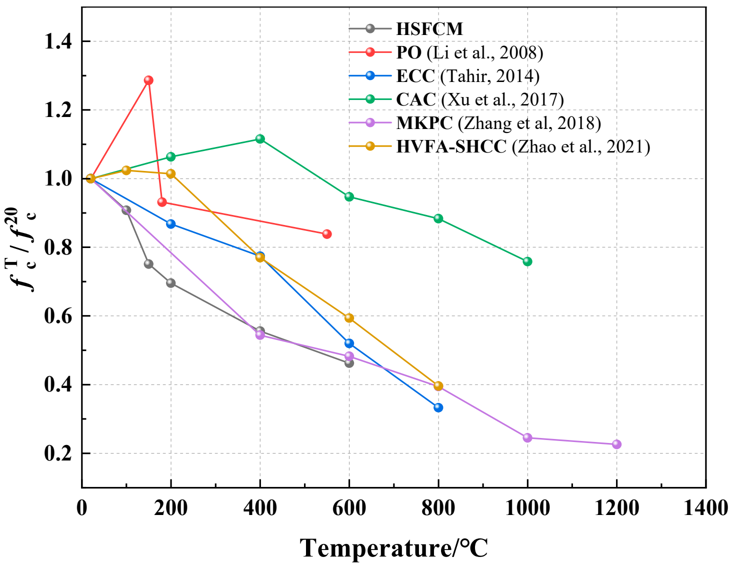

Figure 9. Comparison of compressive strength of several cementitious materials [17,20,37–39].

As can be seen from Figure 9, the influence of high temperature on the compressive strength of different types of cement-based cementitious materials is different. For pure cement cementitious materials such as PO and CAC, the compressive strength tends to rise with the increase of temperature, which may be caused by the continuation of the unfinished hydration reaction due to the increase in temperature. After reaching a certain temperature, the strength begins to decline. For composite cementitious materials composed of a variety of raw materials, the compressive strength is more seriously affected by the deterioration of high temperature, and decreases continuously with the increase of temperature, which is caused by different material components affected by temperature (pyrolysis, chemical reaction, etc.). In general, HSFCM is more deteriorated at high temperature than other materials, because there is more sulfoaluminate cement in the ingredients of HSFCM. Sulfoaluminate cement has a fast setting speed, high early strength and good freezing resistance [40], but it is generally not suitable for high temperature environments [15]. The content of sulfoaluminate cement can be reduced in the follow-up HSFCM high temperature resistance improvement.

4.2. Peak Strain of HSFCM after High Temperature Treatment

Peak strain is an important index reflecting the deformation capacity, which can be used to analyze the deformation law of cement-based cementitious materials [41,42]. The peak strain of HSFCM treated at each temperature is selected from the stress–strain curve, and the ratio of peak strain treated at high temperature ε^{T} to peak strain at room temperature ε^{20} varies with temperature (Figure 10).

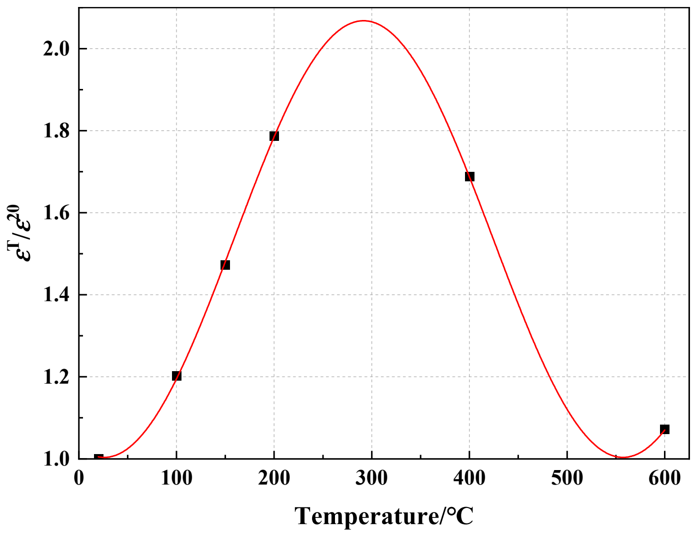

Figure 10. Peak strain ratio changes with temperatures.

The peak strain ratio increases with the increase of temperature within 200 °C. At 400~600 °C, due to severe internal heat damage, the compressive resistance and deformation ability of the specimens deteriorated, and the peak strain showed a downward trend, but all of them were greater than the peak strain at 20 °C. The peak strain ratio obtained from the test was fitted with the temperature, and the relation Equation (1) was obtained from Figure 10:

$$\frac{\varepsilon^{T}}{\varepsilon^{20}} = 0.53\sin\left(\pi\frac{T-159}{266}\right) + 1.54 \tag{1}$$

where T is the treatment temperature. The correlation coefficient R^2 of peak strain ratio and temperature fitting curve is 0.999, indicating a good degree of fitting.

4.3. Elastic Modulus of HSFCM after High Temperature Treatment

Elastic modulus is an index to measure the difficulty of material deformation [43]. It is calculated by referring to Equation (2) in ASTM C 469/C 469M:

$$E = \frac{\sigma_{0.4} - \sigma_1}{\varepsilon_{0.4} - \varepsilon_1} \tag{2}$$

where $\sigma_{0.4}$ is the stress value at 40% of the peak stress; $\varepsilon_{0.4}$ is the strain value corresponding to $\sigma_{0.4}$; and σ_1 and ε_1 are the stress and strain values, respectively, corresponding to 1 kN load.

The elastic modulus was calculated; the ratio of the elastic modulus after high temperature treatment E^{T} and the elastic modulus at room temperature E^{20} changed with temperature (Figure 11).

High temperature decreased the stiffness of HSFCM, the elastic modulus decreased with increasing temperature and the deterioration rate was first rapid and then slowed down. Equation (3) is obtained by fitting the relationship between the ratio of elastic modulus and temperature in Figure 11:

$$\frac{E^{T}}{E^{20}} = \frac{2.56}{T^{0.17}} \tag{3}$$

where T is the treatment temperature. The correlation coefficient R^2 of the elastic modulus ratio of HSFCM to the fitting curve of temperature is 0.991, indicating a good degree of fitting.

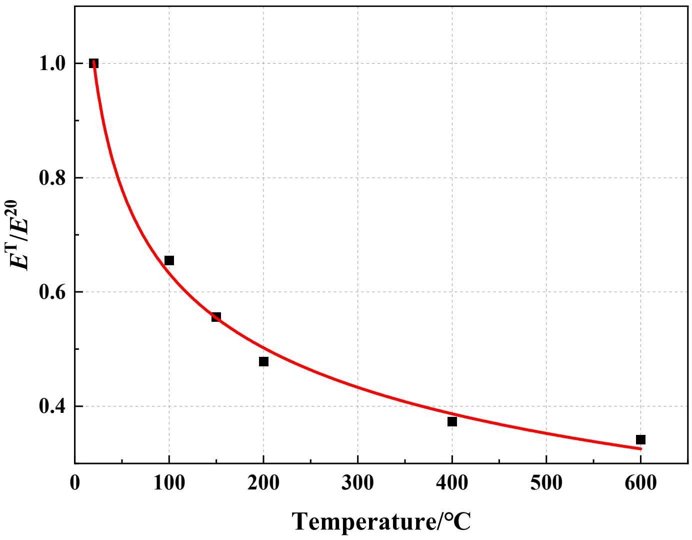

Figure 11. Elastic modulus ratio changes with temperatures.

5. Conclusions

(1) The compressive strength of HSFCM deteriorated after high temperature treatment, and the compressive strength decreased gradually with the increase in temperature. At 100 °C, the compressive strength decreased less; at 100~200 °C, the specimen damage increased and the strength decreased faster; at 400 °C, the compressive strength decreased by more than half. HSFCM is brittle under compression. With the increase of temperature, the peak stress and curve slope decrease, and the growth segment before reaching the peak decreases.

(2) The peak strain of HSFCM increased with increasing temperature at 200 °C, and decreased with increasing temperature at 400~600 °C. High temperature decreased the stiffness of HSFCM, the elastic modulus decreased with increasing temperature and the deterioration rate was first fast and then slow.

(3) A CT scan was used to study the microstructure changes of HSFCM after high temperature treatment, and it was found that the influence of high temperature on HSFCM mainly manifested as the increase of pore number and pore size in three-dimensional space; the high-density material was also gradually decomposed by heat with the increase in temperature.

(4) By comparing XRD patterns, it was found that hydration products such as ettringite and calcium silicate hydrate are gradually decomposed by heat, and multiple diffraction peaks of SiO_2, $CaSO_4$ and CaO appear, indicating that with the increase of temperature, the decomposition of gelling substances in HSFCM becomes more serious, and stable oxides are eventually generated.

(5) Through SEM analysis, it was found that a large number of irregular crystals and whiskers appeared when HSFCM was heated, the cementing material between crystals decreased, the surface bulges and folds gradually became uneven, the honeycomb micropores increased, the pores increased and the micro-cracks developed through each other.

In summary, the changes of microstructure and composition of HSFCM are in good agreement with the experimental results of mechanical properties after high temperature, which is the fundamental reason for the deterioration of its macroscopic mechanical properties at high temperature.

Author Contributions: Methodology, Y.L., Q.M. and Y.Z.; formal analysis, H.P.; investigation, H.P.; data curation, Y.L.; writing—original draft preparation, Y.L.; writing—review and editing, Y.Z. and T.L.; supervision, H.P. and T.L.; project administration, Q.M. and Y.Z.; funding acquisition, Q.M., Y.Z. and T.L. All authors have read and agreed to the published version of the manuscript.

Funding: National Natural Science Foundation of China (U2006213, 42277139, 42207172, 42272327); China Postdoctoral Science Foundation (2022M712989); National Natural Science Foundation of Shandong Province (ZR2022QD103).

Institutional Review Board Statement: Not applicable.

Informed Consent Statement: Not applicable.

Data Availability Statement: The data used to support the findings of this study are included within the article.

Conflicts of Interest: The authors declare no conflict of interest.

References

1. Guo, X.; Liu, Z.; Zheng, J.; Luo, Q.; Liu, X. Bearing capacity factors of T-bar from surficial to stable penetration into deep-sea sediments. *Soil Dyn. Earthq. Eng.* **2023**, *165*, 107671. [CrossRef]
2. Li, C. China cement industry structural adjustment and development report. *China Cem.* **2021**, *2022*, 10–17.
3. Lin, J.; Dong, Y.; Duan, J.; Zhang, D.; Zheng, W. Experiment on single-tunnel fire in concrete immersed tunnels. *Tunn. Undergr. Space Technol.* **2021**, *116*, 104059. [CrossRef]
4. El-Khoury, M.; Roziere, E.; Grondin, F.; Cortas, R.; Chehade, F.H. Experimental evaluation of the effect of cement type and seawater salinity on concrete offshore structures. *Constr. Build. Mater.* **2022**, *322*, 126471. [CrossRef]
5. Guo, X.; Nian, T.; Fu, C.; Zheng, D. Numerical Investigation of the Landslide Cover Thickness Effect on the Drag Forces Acting on Submarine Pipelines. *J. Waterw. Port Coast. Ocean. Eng.* **2023**, *149*, 04022032. [CrossRef]
6. Peng, R.X.; Qiu, W.L.; Teng, F. Research on performance degradation analysis method of offshore concrete piers in cold regions. *Ocean. Eng.* **2022**, *263*, 112304. [CrossRef]
7. Zhou, Y.; Xin, Y.; Zhang, S. Review on recent grave accidents in long tunnels of highway around the world for safety facility. *Chin. J. Rock Mech. Eng.* **2004**, *23*, 4882–4887.
8. Zhang, Z. Research of Mechanics Behavior for Immersed Tuunel under Fire Load. Master's Thesis, Chongqing Jiaotong University, Chongqing, China, 2013.
9. Guo, Q. A Study on Temperature Distribution of Tunnel and Damage of the Lining Structure under High Temperature of Fire. Master's Thesis, Taiyuan University Of Technology, Taiyuan, China, 2015.
10. Hu, X. Study on Structural Fire Safety of Long and Large Subsea Railway Shield Tunnel. Master's Thesis, Southwest Jiaotong University, Chengdu, China, 2021.
11. Yuzer, N.; Akoz, F.; Ozturk, L.D. Compressive strength-color change relation in mortars at high temperature. *Cem. Concr. Res.* **2004**, *34*, 1803–1807. [CrossRef]
12. Feng, J.; Fu, Y.; Chen, Z.; Zhang, R. Effect of high temperatures on microstructure of cement-based composite material. *J. Build. Mater.* **2009**, *12*, 318–322.
13. Zhou, W.; Xu, Z.; Deng, M. High temperature stability of cement containing 20% gypsum sulfoaluminate. *China Concr. Cem. Prod.* **2000**, *5*, 50–53. [CrossRef]
14. Xu, Z.; Zhou, W.; Deng, M. Stability of hardened sulph-aluminate cement paste treated at high temperature. *J. Chin. Ceram. Soc.* **2001**, *29*, 104–108.
15. Xiao, Z.; Lou, Y.; Guo, J. Effect of high temperature drying treatment on properties of sulfoaluminate cement mortar and its mechanism. *Cement* **2018**, *7*, 7–10. [CrossRef]
16. Chowdary, M.; Asadi, S.S.; Poluraju, P. Impact of materials on characteristics of engineered cementitious composite at elevated temperatures: An integrated approach. In Proceedings of the 1st International Conference on Advanced Lightweight Materials and Structures (ICALMS), Hyderabad, India, 6–7 March 2020; pp. 1389–1393.
17. Erdem, T.K. Specimen size effect on the residual properties of engineered cementitious composites subjected to high temperatures. *Cem. Concr. Compos.* **2014**, *45*, 1–8. [CrossRef]
18. Wang, Z.-B.; Han, S.; Sun, P.; Liu, W.-K.; Wang, Q. Mechanical properties of polyvinyl alcohol-basalt hybrid fiber engineered cementitious composites with impact of elevated temperatures. *J. Cent. South Univ.* **2021**, *28*, 1459–1475. [CrossRef]
19. Zhu, J. Basic Research on High Temperature Resistance of Alkali-Activated Slag Cementitious Material and Its Application in Engineering. Ph.D. Thesis, Harbin Institute of Technology, Harbin, China, 2014.
20. Zhao, J.; Niu, M.; Zhou, J.; Wang, Z. Uniaxial compressive behavior and constitutive relationship of HVFA-SHCC after exposure to high temperature. *J. Build. Mater.* **2021**, *24*, 22–30.
21. Su, X.-G.; Du, X.-J.; Yuan, H.-H.; Li, B.-K. Research of the thermal stability of structure of resin anchoring material based on 3D CT. *Int. J. Adhes. Adhes.* **2016**, *68*, 161–168. [CrossRef]

22. Peng, Y.; Zhao, X.; Xu, S.; Li, Q. Microstructure characteristics of ultra-high toughness cementitious composites after exposure to high temperature. *J. Chin. Electron Microsc. Soc.* **2019**, *38*, 236–244.
23. Takahashi, H.; Sugiyama, T. Application of non-destructive integrated CT-XRD method to investigate alteration of cementitious materials subjected to high temperature and pure water. *Constr. Build. Mater.* **2019**, *203*, 579–588. [CrossRef]
24. Guo, X.; Stoesser, T.; Zheng, D.; Luo, Q.; Liu, X.; Nian, T. A methodology to predict the run-out distance of submarine landslides. *Comput. Geotech.* **2023**, *153*, 105073. [CrossRef]
25. Gao, Y. Preparation of Multi-Source Solid Waste Based Marine Grouting Material and Research on Its Performance. Master's Thesis, Shandong University, Shandong, China, 2021.
26. Yang, Z.; Liu, Q.; Huang, X.; Ling, X. Preparation method of high strength fast anchorage agent and its grout. China Patent CN201810739147, 23 November 2018.
27. Liu, Q.; Huang, C.; Liu, L.; Ye, S.; Zang, G.; Gao, W.; Zhang, J. Reinforcement-Mud-Rock bonding test based on FAST-1 new high strength anchoring agent. *J. Jilin Univ.* **2021**, *51*, 1570–1577. [CrossRef]
28. Wang, Y.; Xu, L. Research progress of the influence of particle size distribution on the properties of cement. *Mater. Rep.* **2010**, *24*, 68–71+80.
29. Yi, S.T.; Kim, J.K.; Oh, T.K. Effect of strength and age on the stress-strain curves of concrete specimens. *Cem. Concr. Res.* **2003**, *33*, 1235–1244. [CrossRef]
30. Jia, B. Static and Dynamic Mechanical Behavior of Concrete at Elevated Temperature. Ph.D. Thesis, Chongqing University, Chongqing, China, 2011.
31. Duan, A. Research on Constitutive Relationship of Frozen-Thawed Concrete and Mathematical Modeling of Freeze-Thaw Process. Ph.D. Thesis, Tsinghua University, Beijing, China, 2009.
32. Su, X.; Du, X.; Su, L.; Wang, M.; Yuan, H.; Li, B. Experimental analysis on the micro-structure and the mechanical-properties of resin anchor material at high temperature. *J. China Coal Soc.* **2015**, *40*, 2408–2413. [CrossRef]
33. Su, X.; Du, X.; Zhang, S.; Yang, Z.; Guan, J. Anchoring properties and CT analysis affected by the pyrolysis of the resin anchoring material at high temperature. *Chin. J. Rock Mech. Eng.* **2016**, *35*, 964–970. [CrossRef]
34. Ibrahim, R.K.; Hamid, R.; Taha, M.R. Fire resistance of high-volume fly ash mortars with nanosilica addition. *Constr. Build. Mater.* **2012**, *36*, 779–786. [CrossRef]
35. Wang, G.; Zhang, C.; Zhang, B.; Li, Q.; Shui, Z. Study on the high-temperature behavior and rehydration characteristics of hardened cement paste. *Fire Mater.* **2015**, *39*, 741–750. [CrossRef]
36. Wu, X.; Dai, S.; Li, Z.; Li, W.; Wang, J. Compressive strength and microstructure of cement-based materials after high temperature. *Bull. Chin. Ceram. Soc.* **2019**, *38*, 1755–1758. [CrossRef]
37. Li, Q.; Yao, Y.; Sun, B.; Li, Z. Mechanism of effect of elevated temperature on compressive strength of cement mortar. *J. Build. Mater.* **2008**, *11*, 699–703.
38. Xu, W.; Dai, J.-G.; Ding, Z.; Wang, Y. Polyphosphate-modified calcium aluminate cement under normal and elevated temperatures: Phase evolution, microstructure, and mechanical properties. *Ceram. Int.* **2017**, *43*, 15525–15536. [CrossRef]
39. Zhang, X.; Li, G.; Niu, M.; Song, Z. Effect of calcium aluminate cement on water resistance and high-temperature resistance of magnesium-potassium phosphate cement. *Constr. Build. Mater.* **2018**, *175*, 768–776. [CrossRef]
40. Chen, J. Research of Properties Modification and Applications of Sulphoaluminate Cement. Master's Thesis, Wuhan University, Wuhan, China, 2005.
41. Qin, L. Study on the Strength and Deformation of Concrete under Multiaxial Stress after High-Temperature or Freeze-Thaw Cycling. Ph.D. Thesis, Dalian University of technology, Dalian, China, 2003.
42. Zhang, Z. Experimental Study on the Multi-Axial Mechanical Behavior of Concrete after Freeze-Thaw Cycling or High Temperature. Ph.D. Thesis, Dalian University of Technology, Dalian, China, 2007.
43. Tang, J.; Ma, W.; Pang, Y.; Fan, J.; Liu, D.; Zhao, L.; Sheikh, S.A. Uniaxial compression performance and stress-strain constitutive model of the aluminate cement-based UHPC after high temperature. *Constr. Build. Mater.* **2021**, *309*, 125173. [CrossRef]